Heliyon 10 (2024) e34321

Contents lists available at ScienceDirect

Heliyon

journal homepage: www.cell.com/heliyon

Research article

Synergistic delivery of hADSC-Exos and antioxidants has inhibitory effects on UVB-induced skin photoaging

Yu Fu [a], Jun-ling Xie [a], Wan-ting Zhang [b], Xing-liao Zhang [a], Xin-Min Zhang [b], Meng-meng Xu [a], Yao-ting Han [b], Rong-qi Liu [b], Guang-ming Xie [a], Jing Zhang [b,c,*], Jun Zhang [a,c,d,**]

[a] Research Center for Translational Medicine at East Hospital, School of Medicine, Tongji University, Shanghai, 200010, China
[b] Research Center for Translational Medicine at East Hospital, School of Life Science and Technology, Tongji University, Shangha, 200010, China
[c] Tongji Lifeng Institute of Regenerative Medicine, Tongji University, Shanghai, 200092, China
[d] Shanghai Institute of Stem Cell Research and Clinical Translation, Shanghai, 200092, China

ARTICLE INFO

Keywords:
hADSC-Exos
Antioxidants
Anti-Photoaging
Skin rejuvenation
Synergistic delivery

ABSTRACT

Ultraviolet B (UVB) light exposure accelerates skin photoaging. Human adipose-derived stem cell exosomes (hADSC-Exos) and some antioxidants may have anti-photoaging effects. However, it is unknown whether the combination of hADSC-Exos and antioxidants plays a synergistic role in anti-photoaging. In cellular and 3D skin models, we showed that vitamin E (VE) and hADSC-Exos were optimal anti-photoaging combinations. In vivo, VE and hADSC-Exos increased skin tightening and elasticity in UVB-induced photoaging mice Combined treatment with VE and hADSC-Exos inhibited SIRT1/NF-κB pathway. These findings contribute to the understanding of hADSC-Exos in conjunction with other antioxidants, thereby providing valuable insights for the future pharmaceutical and cosmetic industries.

1. Introduction

Skin aging can be caused by both ultraviolet A (UVA) and ultraviolet B (UVB) radiation; however, UVB is currently considered the key etiological agent [1,2]. Skin photoaging increases skin cancer-causing potential, highlighting the urgent need for active anti-photoaging ingredients [3,4]. Previous evidence suggests that human adipose-derived stem cell exosomes (hADSC-Exos) may attenuate reactive oxygen species (ROS) production and the inflammatory response, thereby improving skin resistance to photoaging [5]. In the cosmetic industry, the inclusion of exosomes in cosmetics is currently a trend in the development of a new generation of over-the-counter cosmetics. On the other hand, various studies had demonstrated the anti-photoaging effects of traditional antioxidants. Nowadays, antioxidants have ripened into a full-fledged mature technology being utilized in numerous everyday applications [6,7]. Idebenone (IDE), chlorogenic acid (CGA), vitamin C (VC), vitamin E (VE), and zinc (Zn) are the most commonly used antioxidant additives [8–12]. IDE, similar to coenzyme Q10, acts as a cell membrane antioxidant. CGA is a natural polyphenol with potent

* Corresponding author. Research Center for Translational Medicine at East Hospital, School of Life Science and Technology, Tongji University, Shanghai, 200010, China.
** Corresponding author. Research Center for Translational Medicine at East Hospital, School of Medicine, Tongji University, Shanghai, 200010, China.
E-mail addresses: 96755@tongji.edu.cn (J. Zhang), 92870@tongji.edu.cn (J. Zhang).

https://doi.org/10.1016/j.heliyon.2024.e34321
Received 20 March 2024; Received in revised form 8 July 2024; Accepted 8 July 2024
Available online 9 July 2024

antioxidant properties. VE in the form of α-tocopherol is a fat-soluble vitamin that functions as an antioxidant. VC is another important antioxidant. ZnO is commonly used in cosmetics and sunscreens owing to its UV absorption ability. Nevertheless, the interaction between hADSC-Exos and antioxidants associated with skin photoaging remains largely unknown. To understand their potential synergy or differences, it is essential to conduct a comprehensive analysis and comparison of their mechanisms.

Our previous study indicated that hADSC-Exos could improve cutaneous wound healing and regeneration, repair collagen fibers, and normalize collagen synthesis in mouse skin [13,14]. Collagen is considered a key factor in skin health because photoaging decreases its presence in the body. To improve the anti-photoaging ability of hADSC-Exos, the objective of this study was to select potential combined treatment antioxidants and evaluate whether their delivery could synergistically protect against UVB-induced photoaging of the skin. Due to its importance and urgency, it will be the catalyst for global anti-photoaging research and exosome industrialization.

2. Materials and methods

2.1. Ethics statements

All procedures followed the guidelines of the National Health and Medical Research Council of China, and approval was obtained from the East Hospital Affiliated to the Tongji University Ethical Review Board.

2.2. hADSCs and exosome extraction

In our previous study, hADSCs were isolated from adipose tissue discarded from patients who underwent liposuction [13–16]. To demonstrate the three-way differentiation capacity of hADSCs, the cells were incubated in chondrogenic, osteogenic, and adipogenic culture media (Saiye Biotechnology Co., Ltd., China). The expression of positive and negative MSC surface markers was evaluated using flow cytometry. hADSCs were used in subsequent analyses from passage 5 (P5) to P10. hADSC-Exos were isolated from the supernatant by ultra-centrifugation. hADSC-Exos were characterized according to their particle diameter and size distribution using electron microscopy and Nanosight (NTA). Anti-CD9, anti-CD63, anti-CD81 antibodies were used to detect exosomes. Prior to the transfection, we empirically determined hADSC-Exos selection concentration of the HaCaT cells to be 100 μg/ml of effective concentration.

2.3. Antioxidants preparation

We identified five antioxidants based on the Comparative Toxicogenomics Database (CTD, https://ctdbase.org/). IDE was purchased from MCE (MCE, China), CGA from Sangon Biotech (Sangon, China), VC from Sangon Biotech (Sangon, China), VE from Sangon Biotech (Sangon, China), and ZnSO4 from Sinopharm Chemical Reagent (Sinopharm, China) [17]. Based on previous studies, the effect concentration of each antioxidant was set at 20 nmol/L [18,19]. The cells were treated with antioxidants alone or antioxidants in combination with hADSC-Exos for 24 h. Subsequent assays were performed after one treatment.

2.4. HaCaT cell and 3D skin model

The HaCaT human keratinocyte cell line was acquired from Shanghai FuHeng Biology Co. A 3D skin model called “EpiDerm” (reconstructed human epidermis) was acquired from Shanghai EPISKIN Biotechnology Co., Ltd (Shanghai, China). According to a previously described method, 3D skin tissues were cultured in six-well plates using 2 mL of EpiKutis medium [20].

2.5. Mice

7-week-old male C57BL/6J mice were obtained from Shanghai Lingchang Laboratory Animal Technology Co. Ltd. (Shanghai, China). Hair on the backs of the mice was completely shaved using an animal shaver. Subsequently, hair was completely removed using a depilatory cream (Veet, Reckitt Benckiser, UK). The dorsal skin of the mice was left bare and measured approximately 3 × 4.5 cm. A black disposable opaque adhesive tape was tightly applied to the skin on the backs of the control group mice to avoid irradiation.

2.6. UVB irradiation

UVB irradiation was performed using a UVB lamp (PL-S 9W/01/2P, Philips, Poland) at a wavelength of 311 nm. The irradiation dose was calculated as follows: UV fluence (mJ/cm^2) = depth-averaged fluence rate (mW/cm^2) × exposure time (s). According to the UVB irradiance parameters, the UV lamp was held at a working distance of 10 cm with a radiation value of 2.22 mw/cm^2. Referring to previous studies, to satisfy an irradiation dose of 350 mJ/cm^2 in HaCaT cells and the 3D skin model, we set the irradiation time to 158 s

Table 1
The primers for IL-6 and GAPDH.

Gene name	Gene type	experiment	Primer (5′-3′)
Gapdh	Total RNA	qRT-PCR Forward	GAGCCCGCAGCCCCCCGCTT
		qRT-PCR Reverse	CCCGGGGCCATCACGCCACAG
IL-6	Total RNA	qRT-PCR Forward	ACTCACCTCTTCAGAACGAATTG
		qRT-PCR Reverse	CCATCTTTGGAAGGTTCAGGTTG

with a single daily dosing [21,22]. Based on the wavelengths for low pressure (LP) UV and medium-pressure (MP) UV, the skin photoaging (SP) mouse model mice were exposed to a dose of 150 mJ/cm^2, and the irradiation time was set to 68 s with a single daily dose. This procedure was repeated weekly for 28 days [23].

2.7. Cell apoptosis

The apoptosis rate was counted by flow cytometry using statistical equipment (Beckman Coulter). HaCaT cells were suspended in binding buffer to obtain single-cell suspensions. Subsequently, they were stained in the dark using 2.5 μL Annexin V-APC as well as 5 μL propidium iodide from BD Biosciences, USA. The percentage of apoptotic cells was determined by flow cytometry after washing with PBS [24].

2.8. SA-β-gal staining

Senescent cells were evaluated using a SA-β-gal staining kit (Beyotime Biotechnology, Haimen, China) according to manufacturer's protocol. After washing twice with DPBS, 96-well plates were incubated with 50 μL of SA-β-gal staining solution at 37 °C overnight. The reagent for staining was prepared by combining 10 μL solution B, 10 μL solution A, 930 μL solution C, and 50 μL of X-gal. After washing three times, the 96-well plates were then incubated with 50 μL SA-β-gal fixative solution overnight in a 37 °C incubator (without CO_2). After washing the cells with 70 % ethanol, blue-stained cells were observed under a microscope [25].

2.9. Cell migration

A wound-healing assay was used to evaluate cellular migration. HaCaT cells were cultured in six-well dishes at a density of 5×10^4 cells/well, resulting in 70 % confluence. The migratory ability of HaCaT cells was determined using a transwell chamber (cat:3422, Corning, USA). Migrated HaCaT cells were treated with a 4 % paraformaldehyde solution for 30 min. Cells that migrated across the membrane were fixed with a 4 % paraformaldehyde solution for 10 min and stained with crystal violet solution (0.1 %). Five random fields were counted using a light microscope (Olympus Corporation, Tokyo, Japan).

2.10. ROS

An ROS Assay Kit (Beyotime Biotechnology, China) was used to measure the intracellular ROS levels. HaCaT cells were suspended in a serum-free medium containing DCFH-DA (1:1000) and incubated in a 37°C-incubator shaker for 20 min. After washing thrice with DMEM, DCF fluorescence was measured using a flow cytometry analyzer [26].

2.11. Inflammation antibody array

Ten types of inflammatory cytokines were measured using the QAH-INF-1 array (Raybiotech, Norcross, GA) following the manufacturer's instructions. The Cy3 signal was estimated using an InnoScan300 microarray scanner (Innopsys, France) at 532 nm [27,28]. Bioinformatics analysis was performed using the GeneCards (https://www.genecards.org/), Human Protein Atlas (https://www.proteinatlas.org/), UniProt (https://www.uniprot.org/), and STRING (https://cn.string-db.org/) databases.

2.12. Histological analysis

Histological examination was conducted on three randomly selected mice from each group. To examine subtle changes in the skin, we conducted hematoxylin and eosin staining of the collected skin samples. Beyond that, immunohistochemistry (IHC) was performed according to the standard IHC protocol. Briefly, after fixing in 4 % paraformaldehyde at 4 °C for 24 h, skin samples were dehydrated by graded alcohol and paraffin emulsion embedded. Then, the slides were deparaffinized. The primary antibodies employed in this study were Rabbit Anti-MMP3 antibody (1:100, Abcam, UK, ab52915), Rabbit Anti-COL17 antibody (1:50, Abcam, UK, ab186415), and Rabbit Anti-TNF-α antibody (1:200, Abcam, UK, ab183218).

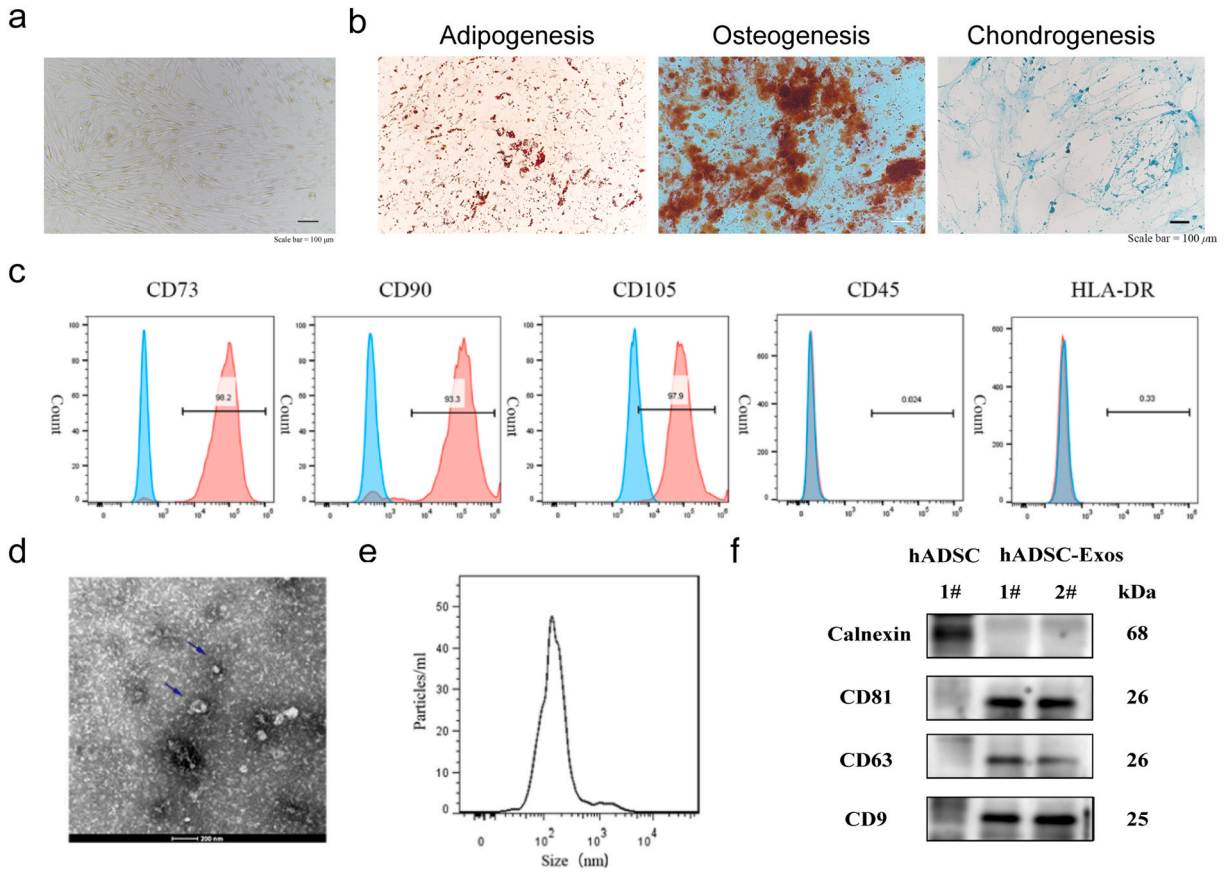

Fig. 1. Identification of the exosome from hADSC. a Morphology of hADSC. Scale bar = 100 μm b multiple differentiation potential of hADSC Scale bar = 100 μm. c Surface markers profiling of hADSC. The cells were highly positive for CD73, CD90, and CD105 and were negative for CD45 and HLA-DR. d. By TEM, purified hADSC-Exo exhibit cup-like morphologies. e Nanoparticle analysis of hADSC-Exo. f. The protein markers in hADSC and hADSC-Exos were analyzed by WB. hADSC expressed Calnexin and hADSC-Exo expressed CD81, CD63, and CD9. Full-length blots/gels are presented in Supplementary original image of the blotting.

2.13. Real-time polymerase chain reaction (qRT-PCR)

The RNeasy Mini Kit (Qiagen, Hombrechtikon, Switzerland) was used to extract total RNA from the tissues and HaCaT cells. qRT-PCR was conducted using the SYBR® Premix Ex TaqTM II Kit (RR820A, Takara Bio, Japan). Using a two-step qRT-PCR technique, the mRNA levels of inflammatory genes were examined. The primers for IL-6 and GAPDH were synthesized by Sangon Biotech (Shanghai, China; Table 1). An ABI7500 qPCR instrument (Applied Biosystems, Oyster Bay, NY, USA) was used for quantitative PCR analysis.

2.14. Western blot (WB)

The following antibodies were applied: Mouse Anti-CD81 antibody (1:1000, Abcam, UK, ab79559), Rabbit Anti-CD63 antibody (1:1000, Abcam, UK, ab134045), Rabbit An-ti-CD9 antibody (1:1000, Abcam, UK, ab92726), Rabbit Anti-Calnexin antibody (1:1000, Abcam, UK, ab22595), Rabbit Anti-SIRT1 antibody (1:1000, Abcam, UK, ab189494), Rabbit Anti-p-p65 antibody (1:1000, Abcam, UK, ab106129), Rabbit Anti-p65 antibody (1:1000, Abcam, UK, ab16502), Rabbit Anti-IL-6 antibody (1:1000, Cell Signaling Technology, USA, 12912), Mouse Anti-GAPDH antibody (1:5000, Abcam, UK, ab8245), goat anti-rabbit IgG-HRP and Cy3-conjugated goat anti-mouse (1:5000, CST, Beverly, MA, USA), and Alexa Fluor®555 goat anti-rabbit IgG (H + L) (1:5000, Invitrogen, Carlsbad, USA). Using the Odyssey Infrared Imaging System, the original membrane images were recorded and analyzed strictly following the ECL WB Protocol (Bio-Rad, Milan, Italy). The original blots with clear edges and marker band sizes were provided in Supplementary file (Supplementary original image of the blotting).

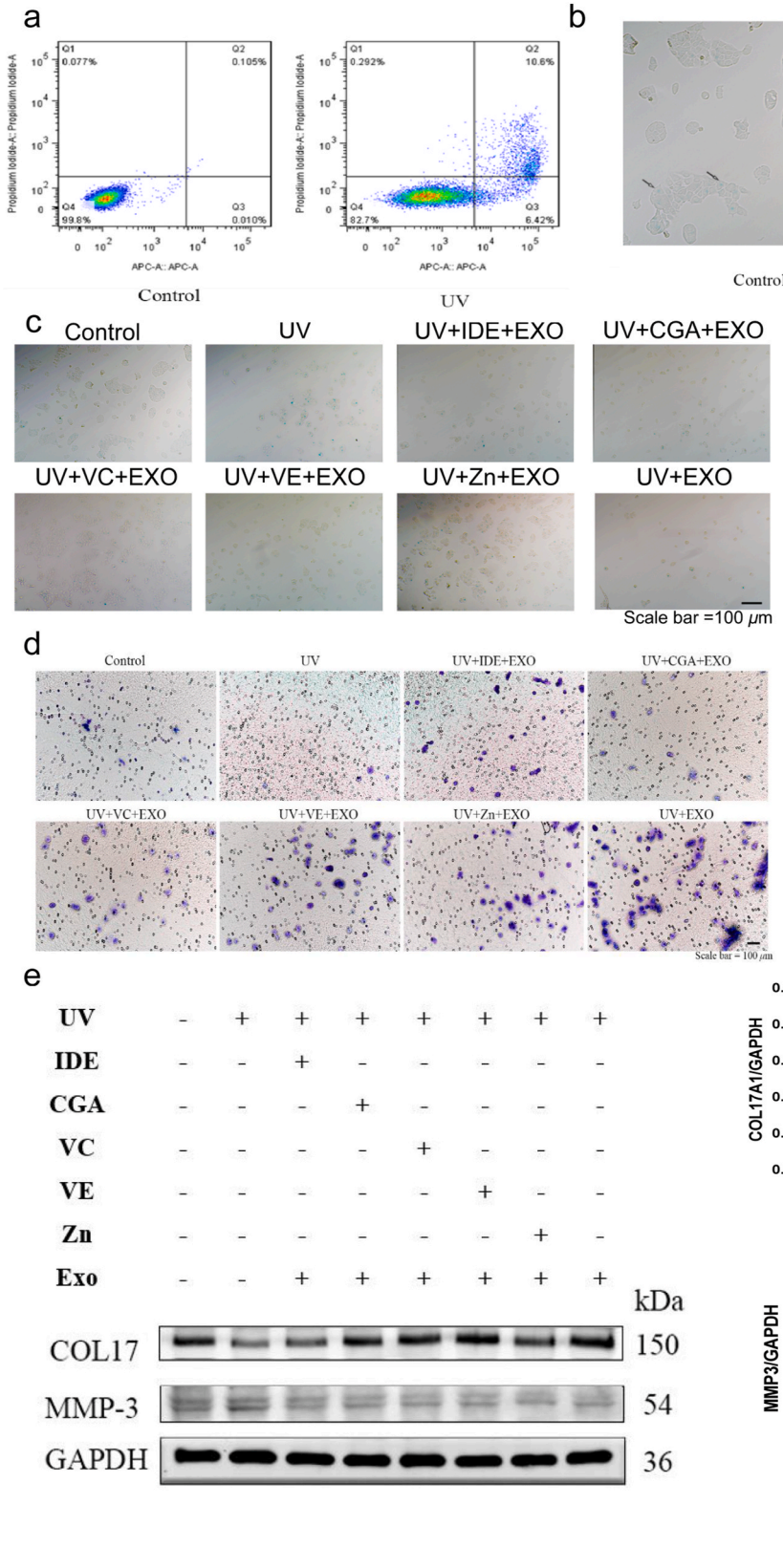

(caption on next page)

Fig. 2. hADSCs-Exo and antioxidants protected HaCaT cells from UVB. a Flow cytometric analysis of apoptotic cells in control group and UV group. b-c Images of senescence-associated SA-β-gal staining of proliferating and senescent HaCaT cells. Control group and UV group (b). hADSCs-Exo and antioxidants protected HaCaT cells from UVB-induced apoptosis in SA-β-gal staining (c). d The migratory properties of HaCaT cells were analyzed using the Transwell migration assay with Transwell filter chambers. e WB Western blot. In UV group, the level of COL17 downregulated and MMP3 levels upregulated by UVB. hADSC-Exo and five antioxidants transfection rescued the expression level of COL17 and MMP3 to different extents. Full-length blots/gels are presented in Supplementary original image of the blotting. Quantification of COL17 and MMP3, normalized to GAPDH levels, and values were plotted. Idebenone (IDE), chlorogenic acid (CGA), vitamin C (VC), VE, zinc (Zn). n = 3. Control, non-exposed HaCaT cells. UV, UVB-exposed HaCaT cells. IDE + EXO, hADSC-Exo and Idebenone-pretreated UVB-exposed HaCaT cells. CGA + EXO, hADSC-Exo and chlorogenic acid-pretreated UVB-exposed HaCaT cells. VC + EXO, hADSC-Exo and vitamin C-pretreated UVB-exposed HaCaT cells. VE + EXO, hADSC-Exo and vitamin E-pretreated UVB-exposed HaCaT cells. Zn + EXO, hADSC-Exo and zinc-pretreated UVB-exposed HaCaT cells. Differences in eight groups were assessed by Tukey's multiple comparison test one-way ANOVA, error bars represent S.E.M. Compared with control group, markered with $*p < 0.05$, $**p < 0.01$, $***p < 0.001$. Compared with UV group, markered with $\#p < 0.05$,$\#\#p < 0.01$,$\#\#\#p < 0.001$,$\#\#\#\#p < 0.0001$.

2.15. Statistical analysis

Statistical analyses were performed using the GraphPad Prism software. In the figure legends, data were presented as the mean ± standard deviation or ± standard error of the mean. A p-value <0.05 was considered statistically significant (confidence interval of 95 %). Two-way or one-way ANOVA was followed by a post hoc Tukey's multiple comparison test. Adobe Illustrator CC software and Figdraw (https://www.figdraw.com/static/index.html) were used to draw a chart of the specific mechanism in this study.

3. Results

3.1. Characterization of hADSC and hADSC-Exos

In our previous studies, we isolated and cultured hADSCs from human adipose tissue [13,14]. Morphological characterization showed that the hADSCs had a typical long spindle morphology (Fig. 1a). We demonstrated that hADSCs have the potential to differentiate into osteoblasts, adipocytes, and chondrocytes, as evidenced by staining with alizarin red S, Oil Red O, and Alcian blue (Fig. 1b). We identified specific marker genes of hADSCs to characterize mesenchymal stem cells (MSCs) by flow cytometry. The P5-10 generation of hADSCs used in this study expressed positive markers of MSCs (CD73, CD90, and CD105) but not negative markers of MSCs (CD45 and HLA-DR, Fig. 1c). hADSC-Exos were examined using transmission electron microscopy and were found to have a typical cup-like structure (Fig. 1d). Using the Zetasizer Nano-Zs analyzer, hADSC-Exos were detected to have a diameter of approximately 140 nm, which falls within the size range criteria for exosomes (30–150 nm, Fig. 1e). Western blotting showed that only hADSCs expressed the endoplasmic reticulum protein calnexin, whereas exosomes did not express calnexin. hADSC-Exos distinctly expressed the exosomal markers CD81, CD63, and CD9 (Fig. 1f).

3.2. hADSCs-Exos and antioxidants protected HaCaT cells against UVB-induced skin photoaging

We chose epidermal HaCaT cells as a cell model for photoaging in vitro. Flow cytometry was performed to determine the effect of UVB irradiation on HaCaT cell apoptosis. The ratio of viable cells decreased and the ratio of apoptotic cells markedly increased after UVB irradiation (Fig. 2a). Compared to that in the control group, UVB exposure remarkably increased both early and late apoptosis in HaCaT cells. There was a 6.41 % increase in early apoptosis, and a 10.495 % increase in late apoptosis. SA-β-gal activity, which is a biomarker of senescence, was detected using SA-β-gal staining. The proportion of SA-β-gal-positive cells showed a marked increase after the UVB treatment (Fig. 2b). This indicated that the cell model for skin photoaging was well established.

Our subsequent investigation focused on the potential of antioxidants and hADSC-Exos in protecting HaCaT cells from UVB-induced apoptosis. Compared to the UV group, VE and hADSC-Exos therapies proved to be the most efficacious (Fig. 2c). HaCaT cell migration was tested by transwell assay. The administration of hADSC-Exos led to elevated cell migration in HaCaT cells, regardless of whether they were administered alone or in combination with antioxidants (Fig. 2d). Lastly, the anti-photoaging marker proteins collagen 17 (COL17) and matrix metalloproteinase 3 (MMP3) were analyzed by WB. The deficiency of COL17 results in premature skin aging by hindering the adhesion of keratinocytes to the underlying membrane [29,30]. MMP3 is an extracellular proteolytic enzyme that cleaves many substrates and is upregulated during senescence and photoaging [31,32]. There were differences between the effects of the different combination of antioxidants and hADSC-Exos. Grossly, the combination of antioxidants and hADSC-Exos was closer to the control group compared to treatment with hADSC-Exos alone. Among them, the combination of hADSC-Exos and VE provided the best performance, since hADSC-Exos and VE treatment resulted in a near-normal level. Compared with treatment of HaCaT cells with UVB, treatment of cells with hADSC-Exos and VE resulted in a significant increase in the expression of the COL17 protein and a reduction in the expression of the MMP3 protein (Fig. 2e). Therefore, the combined delivery of hADSC-Exos and VE protected against UVB-induced skin photoaging.

3.3. Combining hADSC-Exos and VE has the potential to enhance the anti-photoaging effect

Next, we examined the degree of photoaging in HaCaT cells treated with single or combination regimens. All interventions (VE, hADSC-Exos, and hADSC-Exos and VE combination) were significantly superior to the untreated UVB group, and the hADSC-Exos and

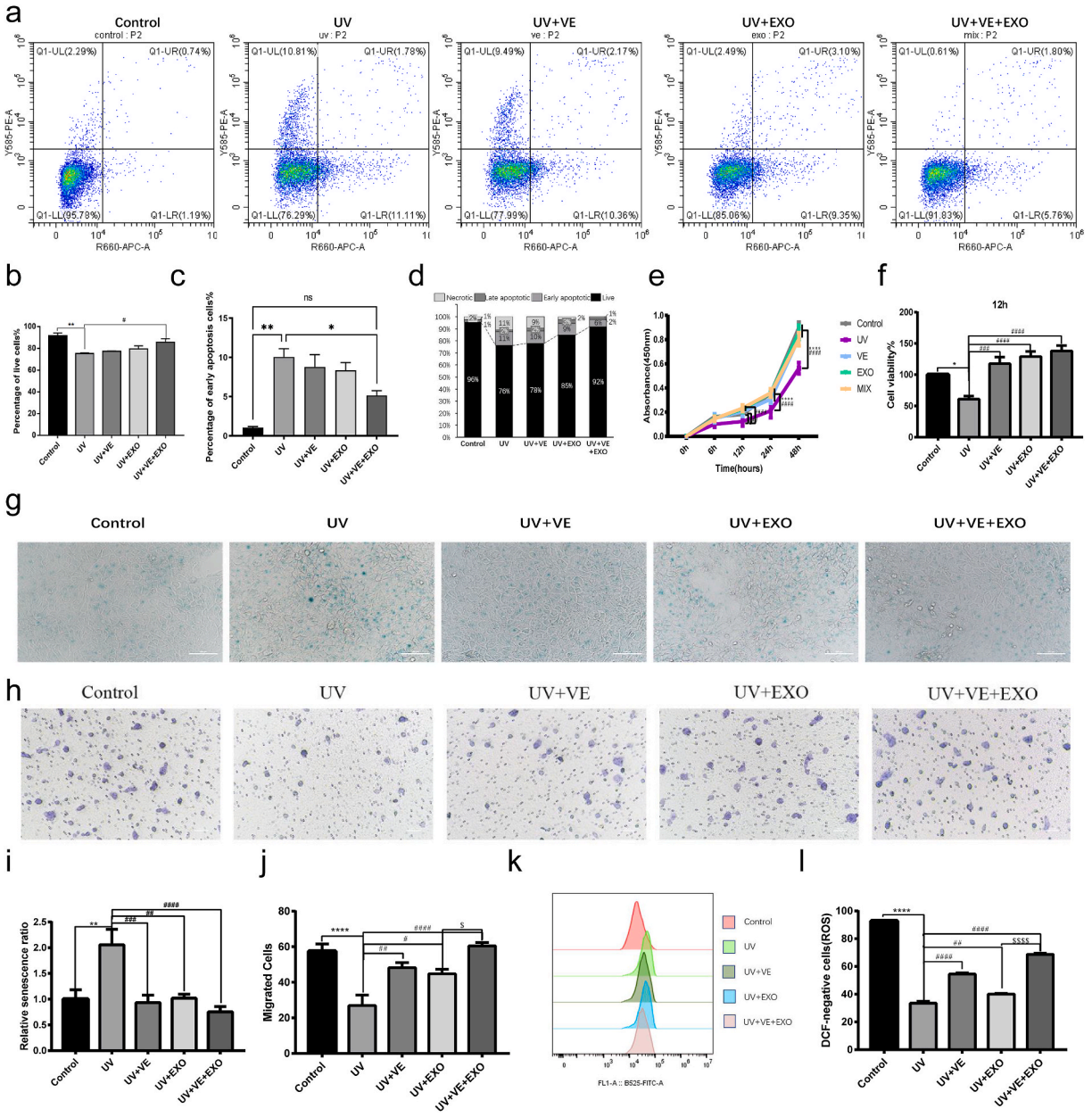

Fig. 3. hADSC-Exo and VE delivery to synergistically against the UVB-induced photoaging in HaCaT cells. a-d Flow cytometric analysis of apoptotic cells in each group. Representative flow cytometric plots (a). b-d Statistical analysis of the results of flow apoptosis experiments in each group. The percentage of live cells (b). The percentage of early apoptosis cells (c). The stacked bar graphs indicate the mean percentage of viable, early apoptotic, and late apoptotic cells (d). e-f CCK8 assay. CCK8 assay was carried out to measure the cell growth in 48 h (e). Cell survival was determined by the CCK8 assay at 12 h (f). g and i SA-β-gal staining. Senescent cells showed a blue staining (g). Statistics of senescence in shown (i). h and j Transwell migration assay. Transwell migration image in each group (h). Quantification of transwell migration assay data (j). k and l ROS. Representative graphs of flow cytometry analysis for ROS levels in HaCaT cells (k). Detection of ROS level in HaCaT cells by DCF fluorescence (l). n = 3. Control, non-exposed HaCaT cells. UV, UVB-exposed HaCaT cells. UV + VE, VE-pretreated UVB-exposed HaCaT cells. UV + EXO, hADSC-Exo-pretreated UVB-exposed HaCaT cells. UV + VE + EXO, hADSC-Exo and VE-pretreated UVB-exposed HaCaT cells. Differences in five groups were assessed by Tukey's multiple comparison test one-way ANOVA, error bars represent S.E.M. Compared with control group, markered with $^{*}p < 0.05$, $^{**}p < 0.01$, $^{***}p < 0.001$. Compared with UV group, markered with $\#p < 0.05$,$\#\#p < 0.01$,$\#\#\#p < 0.001$,$\#\#\#\#p < 0.0001$. Compared with UV + EXO group, markered with \$ $p < 0.05$,\$\$ $p < 0.01$,\$\$\$ $p < 0.001$,\$\$\$\$ $p < 0.0001$.

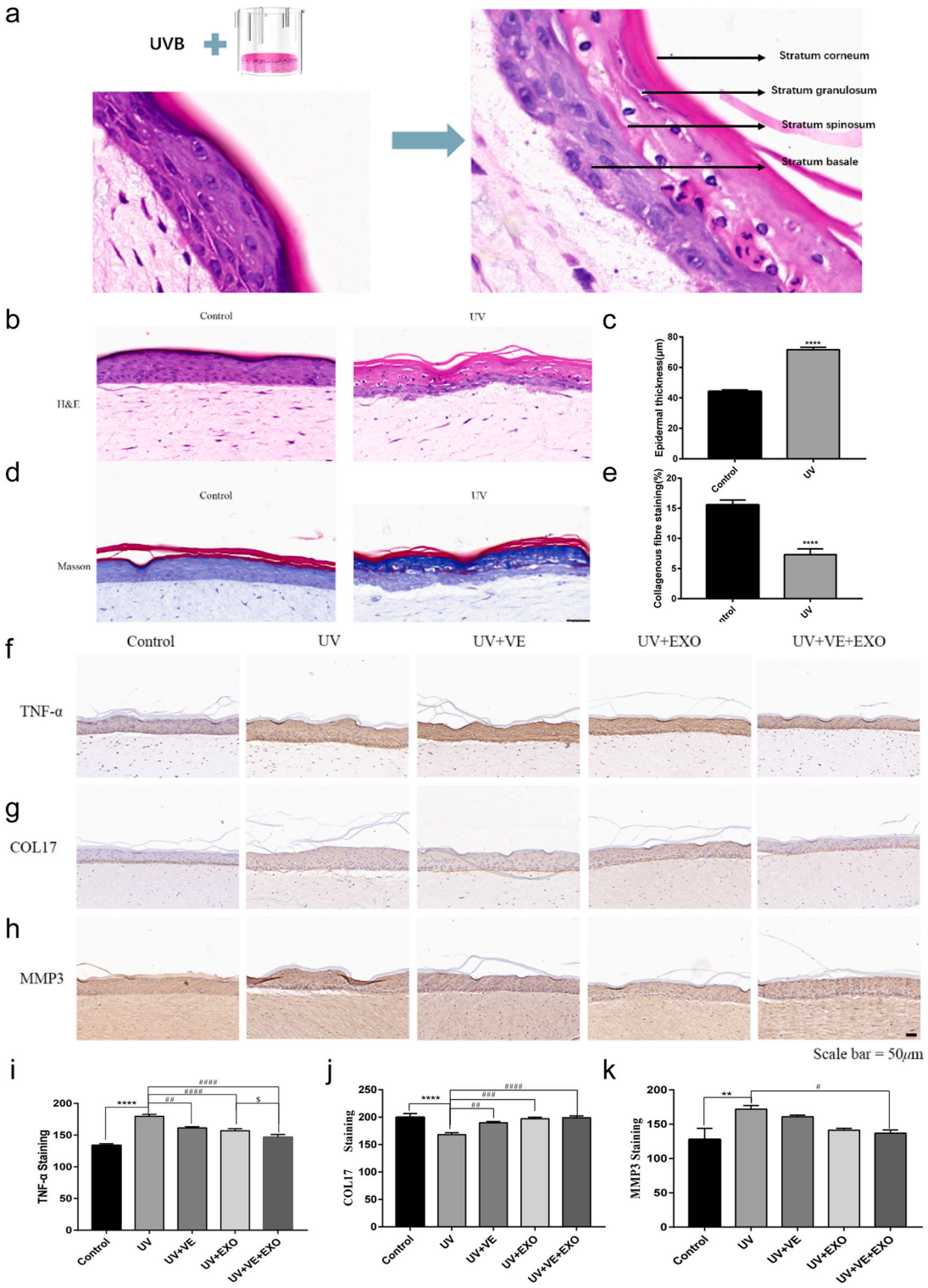

Fig. 4. hADSC-Exo and VE delivery to synergistically against the UVB-induced photoaging in 3D skin model. a-c HE staining of 3D skin model. Representative images in 3D skin model constructs. Stratum Basale (SB), Stratum Corneum (SC), Stratum Granulosum (SG), Stratum Spinosum (SS). (a). Analysis of the thickness of the epidermal layer of 3D skin model in HE staining sections (b). Thickness quantifications of the stratum epidermis (c). d-e Masson staining. Representative images in collagen deposition (blue, d). Quantification of 3D skin model for fibrosis with representative Masson trichrome image (e). f and i Representative photographs of TNF-α, immunostaining. Scale bar = 50 μm (f). Quantitative analysis of TNF-α (i). g and j Representative photographs of COL-17, immunostaining. Scale bar = 50 μm (g). Quantitative analysis of COL-17 (j). h and k

Representative photographs of MMP3, immunostaining. Scale bar = 50 μm (h). Quantitative analysis of MMP3 (k). Control, non-exposed 3D skin model. UV, UVB-exposed 3D skin model. UV + VE, VE-pretreated UVB-exposed 3D skin model. UV + EXO, hADSC-Exo-pretreated UVB-exposed 3D skin model. UV + VE + EXO, hADSC-Exo and VE-pretreated UVB-exposed 3D skin model. Differences in five groups were assessed by Tukey's multiple comparison test one-way ANOVA, error bars represent S.E.M. Compared with control group, markered with $^{*}p < 0.05$, $^{**}p < 0.01$, $^{***}p < 0.001$. Compared with UV group, markered with $\#p < 0.05$,$\#\#p < 0.01$,$\#\#\#p < 0.001$,$\#\#\#\#p < 0.0001$.

VE combination appeared to be significantly superior to the individual treatments (Fig. 3a). The combination of hADSC-Exos and VE significantly improved protection against apoptosis (Fig. 3b–d). To investigate the effects of hADSC-Exos and VE on HaCaT cell proliferation, we performed a CCK-8 assay (Fig. 3e). At 12 h, HaCaT cell viability was increased by hADSC-Exos and VE compared with that in the UVB group without treatment (Fig. 3f). The combination of hADSC-Exos and VE demonstrated exceptional therapeutic effectiveness in safeguarding against cellular senescence, as indicated by the β-galactosidase staining (Fig. 3g–i). Efficient migration of keratinocytes is essential for restoring the denuded epithelial layer. Although VE and hADSC-Exos increased cell migration, their combined effect was greater, as demonstrated by the transwell assay (Fig. 3h–j). Quantification of the ROS levels indicated a substantial increase in ROS following UVB therapy (Fig. 3k). However, pretreatment with hADSC-Exos and VE prevented this increase. Crucially, combined treatment with hADSC-Exos and VE was more effective in reducing ROS than either treatment alone (Fig.3l). These results indicate that combined treatment with hADSC-Exos and VE offers superior anti-photoaging effects compared to single-agent treatments.

3.4. hADSC-Exos and VE combined treatment against UVB-induced photoaging in human 3D skin model

The human 3D skin model exhibited irregular thickening of the epidermis and loosening of dermal-epidermal adhesions following exposure to UVB. Additionally, the stratum spinosum and granulosum exhibited intracellular vacuolization and pyknotic nuclei. The adhesion between the basal layer and dermis decreased, whereas the number of melanin granules in the mucosal basal layer increased (Fig. 4a–c). Masson's trichrome staining revealed that collagen levels in the UVB group were marked reduction compared with those in the control group (Fig. 4d and e). The skin inflammation induced by UVB radiation exhibited significant increases in skin thickness, infiltration of inflammatory cells, and concentrations of proinflammatory cytokines, such as TNF-α. In the human 3D skin model, the combined treatment of hADSC-Exos and VE restored the expression of TNF-α, COL17A1, and MMP3 to nearly normal levels (Fig. 4f–k). Consequently, hADSC-Exos and VE were delivered synergistically to protect against UVB-induced skin photoaging in a human 3D skin model.

3.5. hADSC-Exos and VE delivery to synergistically protect against UVB-induced photoaging in vivo

To elucidate the anti-photoaging efficacy of hADSC-Exos and VE in vivo, a SP mouse model was used (Fig. 5a). The back of the mouse was shaved, with a 3 × 4.5 cm area of bare skin (Fig. 5b). Skin swelling, thickening, and disorganization in the arrays of collagen and elastin fibrils were observed in the skin of the UV group by HE and Masson staining (Fig. 5c–f). The combination of hADSC-Exos and VE effectively rescued senescence-associated secretory phenotypes (SASP). Skin density and moisture content are crucial parameters for evaluating aging skin [33]. We analyzed the moisture content of the mouse skin using a Real Bubee skin tester (Fig. 5g). Analysis of the moisture content showed a significant decrease in the moisture content of the dorsal skin after a 28-day exposure to UVB. There was an improvement in skin moisture content after combined hADSC-Exos and VE treatment. In the SP mouse model, the expression of TNF-α, COL17, and MMP3 was restored to a near-normal level after combined treatment with hADSC-Exos and VE (Fig. 5h-m). The combined treatment protected against UVB-induced photoaging in vivo.

3.6. Bioinformatics analysis to identify anti-photoaging protein in hADSC-Exos

According to the CTD database, VE assumes a crucial function in skin disorders by modulating the expression of nine genes, including IL-6, CXCL2, and TNF (Fig. 6a). Therefore, we performed an inflammation antibody array to assess changes in human inflammatory factors after UVB exposure (Fig. 6b). Bubble plots and thermograms showed that the UV group exhibited more significant upregulation of IL-6 expression than the control group, as observed in the HaCaT cell culture medium (Fig. 6c and d). GO analysis revealed that compared to the control group, the medium of the UV group displayed notable enrichment in the regulation of oxidoreductase activity, positive regulation of interleukin-6 production, promotion of cytokine formation, positive regulation of cellular activation, and acute inflammatory response (Fig. 6e). The protein expression of the inflammatory factor IL-6 was significantly downregulated after VE treatment (Fig. 6f). Therefore, we hypothesized that VE can decrease the expression of IL-6 and that the inclusion of hADSC-Exos further enhances the anti-photoaging effects of VE. We previously identified 232 active proteins in hADSC-Exos by mass spectrometry (data not shown). To identify the proteins associated with photoaging, the GeneCards, Human Protein Atlas, and UniProt databases were used to retrieve clusters of proteins associated with photoaging. By examining the intersections with 232 active proteins, it revealed that 15 active proteins were detected within hADSC-Exos and were associated with photoaging in Wayne's analysis (Fig. 6g and h). The main functions of these active proteins are protein modification, the cell cycle, cellular metabolism, and cytoskeletal function. Among them, stratifin (SFN) is a member of the 14-3-3 protein family, commonly referred to as 14-3-3σ [34]. The 14-3-3 protein family exerts cytoprotective effects by regulating SIRT1-dependent antioxidant pathways [35]. Protein interactions among SFN, SIRT1, and IL-6 were predicted using the STRING website (Fig. 6i). These findings indicate that SFN derived

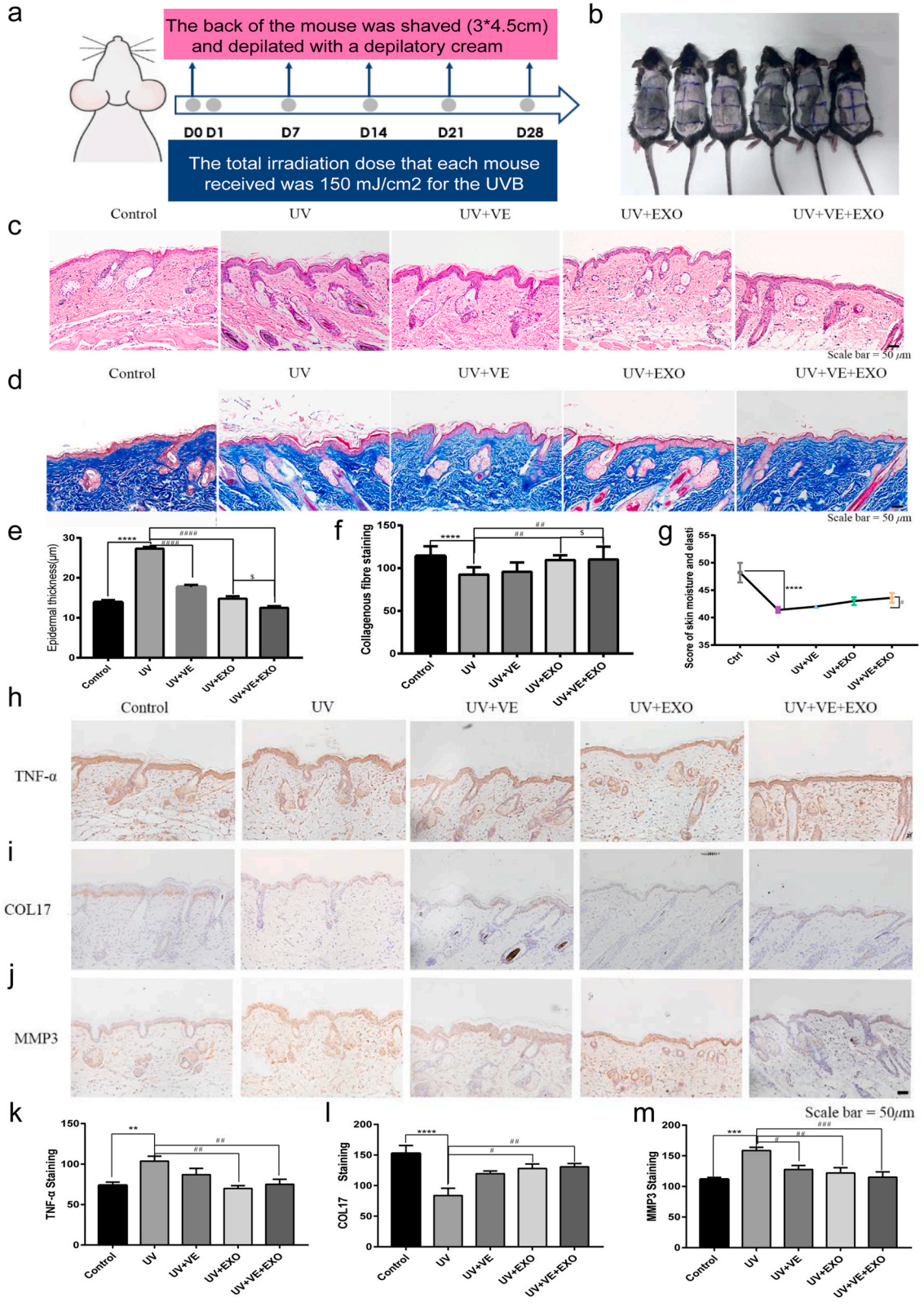

(caption on next page)

Fig. 5. hADSC-Exo and VE delivery to synergistically against the UVB-induced photoaging in photoaged mouse model. a Schematic flowchart of the experiment of UVB-exposed and shaved in photoaged mouse model. b The gross appearances of skin damaged by photoaging in each group. Mice were randomly grouped. Six animals were in each group. c and e HE staining of photoaged mouse model. Representative images in photoaged mouse model constructs (c). Thickness quantifications of the stratum epidermis of photoaged mouse model in HE staining sections (e). d and f Masson staining. Representative images in collagen deposition (blue, d). Quantification of photoaged mouse model for fibrosis with representative Masson trichrome image (f). g The changes of skin moisture content of the photoaged mouse model. h and k Representative photographs of TNF-α, immunostaining. Scale bar = 50 μm (h). Quantitative analysis of TNF-α (k). i and l Representative photographs of COL-17, immunostaining. Scale bar = 50 μm (i). Quantitative analysis of COL-17 (l). j and m Representative photographs of MMP3, immunostaining. Scale bar = 50 μm (j). Quantitative analysis of MMP3 (m). Control, non-exposed photoaged mouse skin. UV, UVB-exposed photoaged mouse skin. UV + VE, VE-pretreated UVB-exposed photoaged mouse skin. UV + EXO, hADSC-Exo-pretreated UVB-exposed photoaged mouse skin. UV + VE + EXO, hADSC-Exo and VE-pretreated UVB-exposed photoaged mouse skin. Differences in five groups were assessed by Tukey's multiple comparison test one-way ANOVA, error bars represent S.E.M. Compared with control group, markered with $*p < 0.05$, $**p < 0.01$, $***p < 0.001$. Compared with UV group, markered with $\#p < 0.05$,$\#\#p < 0.01$,$\#\#\#p < 0.001$,$\#\#\#\#p < 0.0001$. Three mice were randomly selected from each group for histological examination.

from hADSC-Exos may exert photoprotective effects against VE by influencing SIRT1-related inflammation and immunity signaling pathways.

3.7. hADSC exosomal SFN regulates the NF-κB signaling pathway by targeting SIRT1

Some studies have demonstrated that Sirt1 suppresses the acetylation levels of p65 and NF-kB signaling, with the result that the inflammation triggered by NF-κB is diminished [36]. Therefore, we analyzed the expression of key proteins including SIRT1, p-p65, p65, and IL-6 in HaCaT cells. After hADSC-Exos and VE treatment, SIRT1 increased, whereas p-p65, p-65, and IL-6 decreased compared to those in the non-treated UVB group (Fig. 7a and b). Next, we investigated whether SFN could play a role in activating SIRT1 as hADSC-Exos. The expression of SIRT1 was significantly reduced by UVB irradiation in HaCaT cells, which was rescued by SFN overexpression (Fig. 7c and d). Thus, hADSC-Exos and VE inhibited photoaging via the SIRT1/NF-κB pathway (Fig. 7e).

4. Discussion

Skin aging is caused by both intrinsic and extrinsic factors. Extrinsic aging mainly refers to photoaging, which affects quality of life and can even lead to skin cancer [37]. Skin photoaging is caused by UV radiation, particularly UVB radiation. Therefore, we focused primarily on UVB irradiation. UVB radiation accounts for approximately 5 % of the UV radiation present on the Earth's surface and can permeate through the epidermis and upper dermis [38]. To enhance the resistance of the skin to UV rays, several active ingredients such as ZnO have been incorporated into commercial sunscreens and lotions [39]. There is evidence that VE can attenuate UV-induced damage to dermal fibroblasts and epidermal keratinocytes, thus demonstrating its ability to act as a protective agent against UV radiation in the skin [40]. Optimal topical delivery of cosmetic ingredients can be achieved using liposomes [41]. Liposome membranes protect exosomes from degradation or destruction [42]. Small extracellular vesicles derived from young adipose-derived stem cells reduce epigenetic age in old mice [43]. The potential anti-photoaging properties of hADSCs and their exosomes have been explored in several studies [5,44–46]. However, the interactions between hADSC-Exos and other antioxidants remain largely unknown. This limits the further application of hADSC-Exos for anti-photoaging. Therefore, we screened the CTD database to identify the optimal antioxidant that could modulate the anti-photoaging effect of hADSC-Exos. Using bioinformatics analysis, we successfully identified 15 active proteins in hADSC-Exos that are closely related to the photoaging process. In addition, we demonstrated that exosomal SFN extracted from hADSC effectively counteracted skin photoaging through the SIRT1-NF-κB signaling pathway. SIRT belongs to the NAD + -dependent enzyme family, and mammalian SIRT has seven members (SIRT1-7), that are well known for their longevity [47]. According to Wang et al., SIRT6 overexpression regulates the NRF2/HO-1 and NF-kB signaling pathways in skin fibroblasts to alleviate UVA-induced photoaging [48]. SRIT1 may also be a promising target for reducing UV-induced skin aging.

Based on the close correlation between antioxidants and anti-photoaging, various studies have demonstrated the anti-photoaging effects of traditional antioxidants that have been applied in moisturizers, masks, and serums [19,49,50]. Exosomes and antioxidants share some similarities in their mechanisms: (1) Anti-inflammatory properties: both exosomes and antioxidants can inhibit the proliferation of peripheral blood mononuclear cells and downregulate inflammatory cytokines; (2) ROS inhibitory properties: during the photoaging process, exosomes and antioxidants can activate Nrf2 and attenuate the NF-κB pathway; and (3) proliferation-promoting properties: both exosomes and antioxidants promote the proliferation and migration of fibroblasts and keratinocytes [51]. Based on the functional similarity between the two, a future trend is to use both exosomes and antioxidants in cosmetics [52]. Our study shows that the combination of hADSC-Exos and antioxidants has inhibitory effects on the skin photoaging induced by UVB irradiation. Other than that, we reveal the synergistically effect of hADSC-Exos and VE against the UVB-induced photoaging of the skin through the NF-κB signaling pathway via SIRT1. We validated this synergistically effect of hADSC-Exos and VE using a variety of experimental models.

a

	Chemical	Disease	Direct Evidence	Enrichment Analysis	Inference Network	Inference Score	References
201.	alpha-Tocopherol	Kidney Neoplasms			8 genes: ABCB1 | CCND1 | CYP1A1 | GSTT1 | MAPK1 | MAPK3 | PTGS2 | SOD2	16.37	7
202.	alpha-Tocopherol	Marfan Syndrome			4 genes: CAT | NOS2 | SOD1 | SOD2	16.23	1
203.	alpha-Tocopherol	Berylliosis			4 genes: GCLM | IL6 | TGFB1 | TNF	16.22	7
204.	alpha-Tocopherol	Manganese Poisoning			5 genes: IFNG | IL1B | NOS2 | SNCA | TNF	16.10	4
205.	alpha-Tocopherol	Epilepsy			9 genes: ABCB1 | AKT1 | ALB | BDNF | FOS | FOSB | GFAP | SLC1A2 | TGFB1	16.04	11
206.	alpha-Tocopherol	Skin Diseases			9 genes: CXCL2 | GSTM1 | HSPA1B | IL1A | IL1B | IL6 | PTGS2 | SOD2 | TNF	15.90	4

b

c

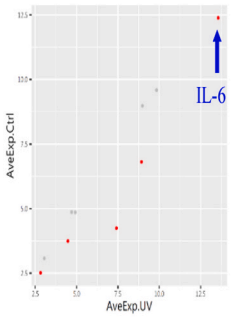

d

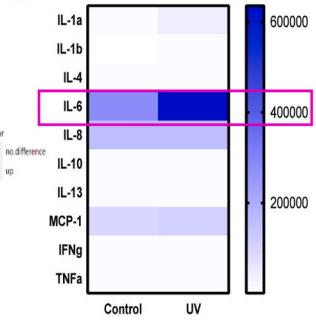

e

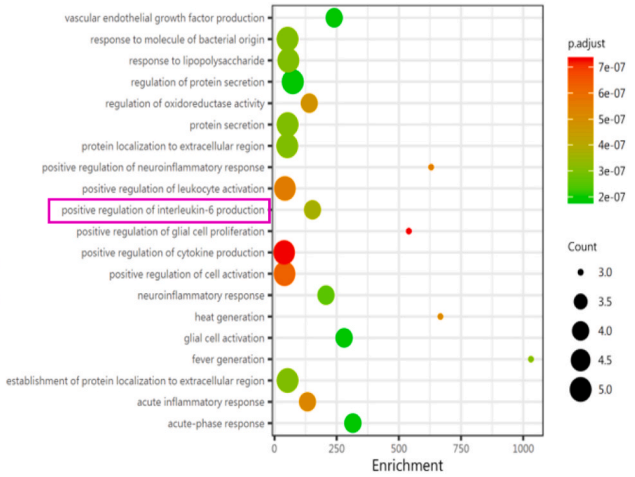

f

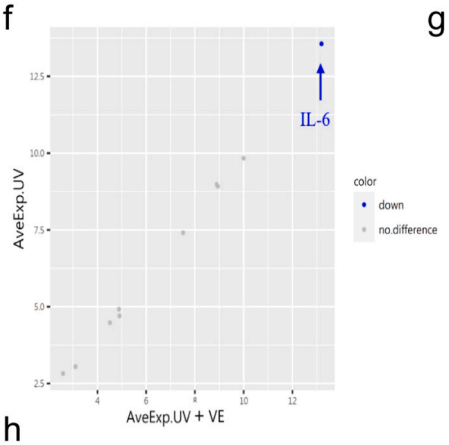

g

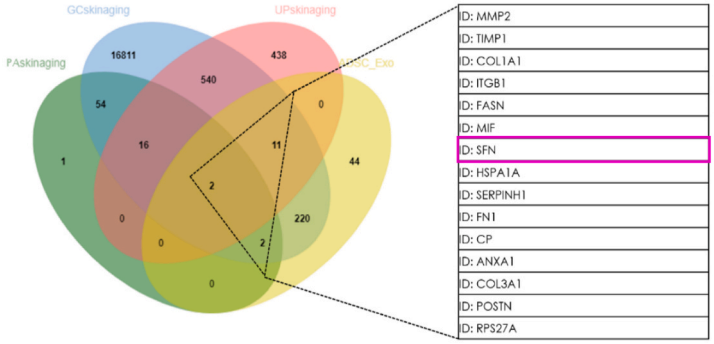

h

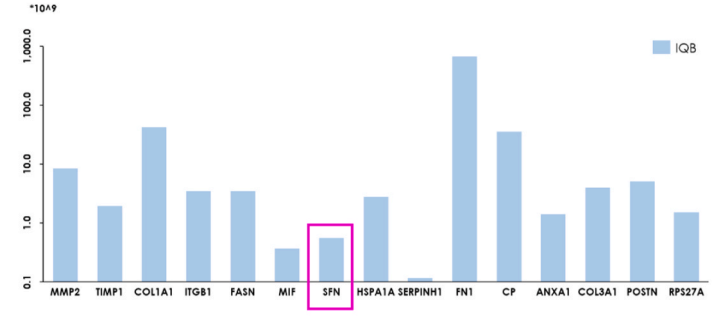

i

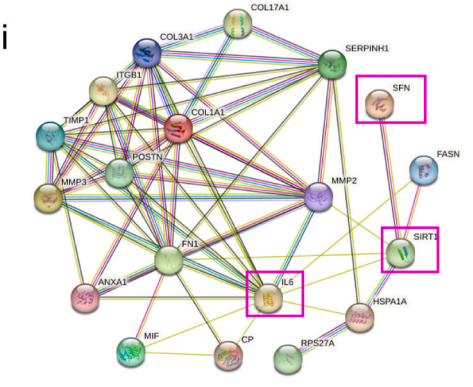

(caption on next page)

Fig. 6. Integrated bioinformatics analysis to identify anti-skin photoaging protein in hADSC-Exo. a The CTD analysis between potential key genes and diseases. b The up panel is a schematic representation of human inflammation antibody array containing 40 inflammation antibodies. c The color of the bubble indicates whether the pathway was upregulated (red) or no difference (gray) and the size of the bubble indicates to the degree of regulation. IL-6 is the most affected among the up-regulated inflammation factors after UVB exposure. d Heat map of the inflammatory cytokines. e UVB actives the signal pathway of related inflammatory factors. f VE modulated the IL-6 to alleviate inflammation. g Wayne diagram displaying the hub photoaging proteins in hADSC-Exo. h Photoaging-related protein abundance identified by mass spectrometry in the hADSC-Exo. i STRING network analysis of the photoaging-related protein interaction network.

Despite promising preclinical data, it is difficult to extrapolate findings from cell cultures and animal models to the complexity of human biology because physiological and pathological conditions may affect exosome function. Because exosomes are rapidly cleared in *vivo*, animal and human studies are necessary to understand their safety, efficacy, dosing, and delivery [53]. Therefore, it is critical to use multiple skin models to elucidate the mechanisms of photoaging. We found that the combination of hADSC-Exos and VE exhibited superior efficacy in safeguarding against skin photodamage at various levels in the cell model, human 3D skin model, and photoaged mouse model. MMPs are responsible for the normal conversion of type I collagen fibers into the extracellular matrix. The two most highly secreted MMPs are MMP1 and MMP3. Recently, MMP3 was identified as a senescence associated secretory phenotype (SASP) factor [54]. Human epidermal aging may be associated with reduced COL17A1 expression COL17A1 expression decreases significantly with epidermal aging, resulting in the loss of dermal-epidermal junctions and a thinner epidermis [55]. COL17A1 is a transmembrane protein of the collagen family that is associated with epithelial cell development and cell cycle. COL17A1 has also been reported to play an important role in many malignant tumors by promoting cancer cell proliferation and invasion. Therefore, it may be better to have a near-normal expression. The expression of COL17 in the VE and hADSC-Exos treatment groups was closer to that observed in the control group, which confirmed the above conclusion. These important findings not only contribute to the existing research in this field but also highlight the combined use of hADSC-Exos and VE as a promising strategy to counteract UV-induced photoaging of the skin. Consequently, our findings suggest a novel combinatorial approach that could provide protection against UVB-induced photoaging and may contribute to potential therapeutic strategies for the treatment and prevention of skin photoaging.

5. Conclusions

In this study, UVB-induced skin photoaging was effectively combined with hADSC-Exos and antioxidant delivery in cellular, 3D skin, and SP mouse models. The combination of hADSC-Exos and VE displayed the best synergistic anti-photoaging effect. Treatment with hADSC-Exos and VE significantly inhibited activation of the NF-κB pathway. hADSC exosome-derived SFN and VE improved photoaging by targeting SIRT1.

Ethics statement

The study received approval from the Committee of Ethics on Experimentation of Tongji University (Shanghai, China), with the ethics approval number TJAA09523102.

Funding

The Peak Disciplines (Type IV) of Institutions of Higher Learning in Shanghai and the China Postdoctoral Science Foundation (2022M722409).

Data availability statement

The data used to support the findings of the present study are available from the corresponding author upon request.

Author information

Yu Fu and Jun-ling Xie contributed equally to this study.

CRediT authorship contribution statement

Yu Fu: Writing – review & editing, Writing – original draft, Methodology, Funding acquisition. **Jun-ling Xie:** Writing – review & editing, Formal analysis, Data curation. **Wan-ting Zhang:** Methodology, Data curation. **Xing-liao Zhang:** Methodology, Conceptualization. **Xin-Min Zhang:** Formal analysis. **Meng-meng Xu:** Investigation. **Yao-ting Han:** Software. **Rong-qi Liu:** Data curation. **Guang-ming Xie:** Data curation. **Jing Zhang:** Writing – review & editing, Validation, Supervision, Funding acquisition. **Jun Zhang:** Visualization, Supervision, Resources, Funding acquisition.

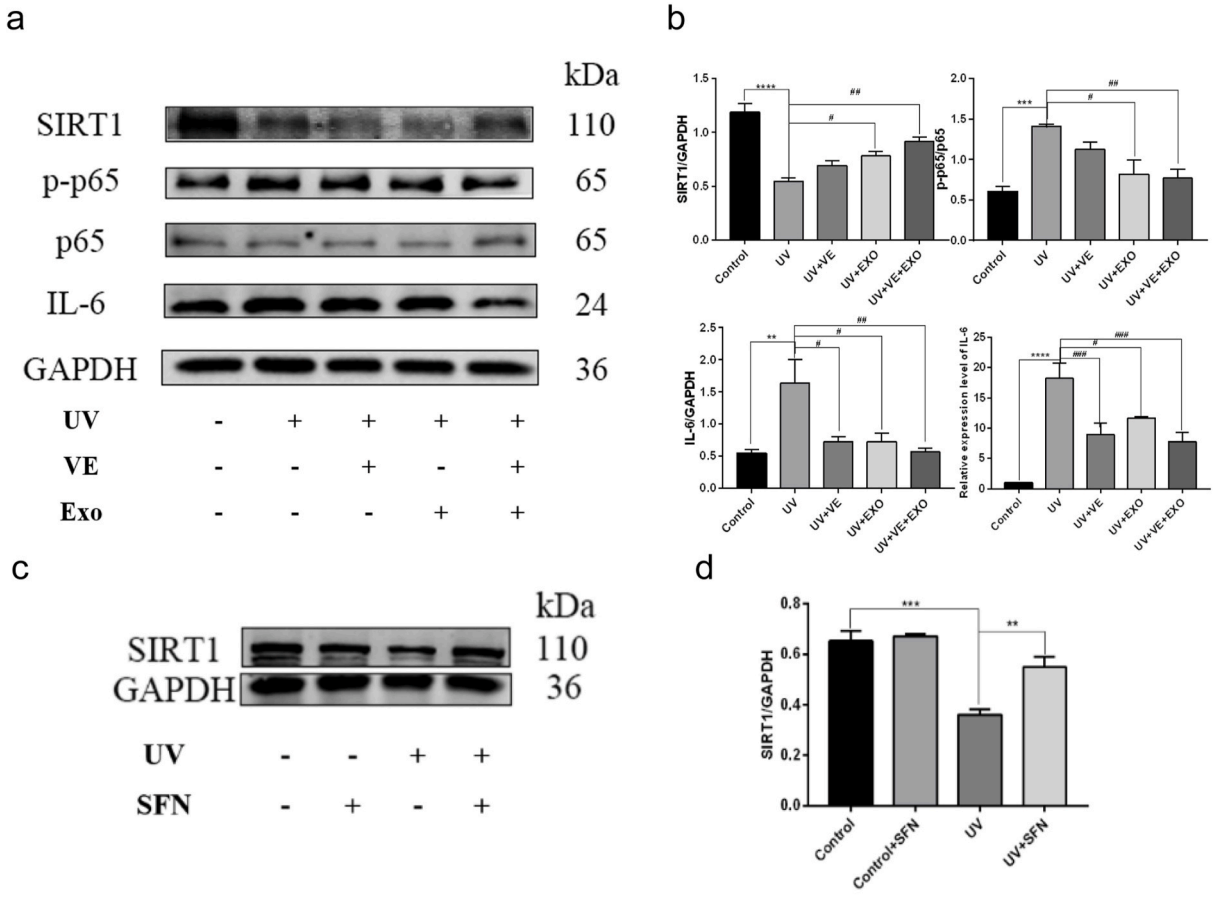

(caption on next page)

Fig. 7. The anti-skin photoaging function of hADSC exosomal SFN via a NF-κB signaling pathway is regulated by SIRT1. a and b Representative WB image of SIRT1, p-p65, p65 and IL-6 in each group (a). Quantitative analysis (b). c and d Representative WB image of SIRT1 after SFN overexpressed in HaCaT cells. Full-length blots/gels are presented in Supplementary original image of the blotting. WB Quantitative analysis and IL-6 quantification was performed by qPCR (d). e Schematic illustration of the role of hADSC-Exo and VE on protecting skin photoaging. n = 3. Control, non-exposed HaCaT cells. UV, UVB-exposed HaCaT cells. UV + VE, VE-pretreated UVB-exposed HaCaT cells. UV + EXO, hADSC-Exo-pretreated UVB-exposed HaCaT cells. UV + VE + EXO, hADSC-Exo and VE-pretreated UVB-exposed HaCaT cells. Differences in five groups were assessed by Tukey's multiple comparison test one-way ANOVA, error bars represent S.E.M. Compared with control group, markered with $*p < 0.05$, $**p < 0.01$, $***p < 0.001$. Compared with UV group, markered with $\#p < 0.05$,$\#\#p < 0.01$,$\#\#\#p < 0.001$,$\#\#\#\#p < 0.0001$.

Declaration of competing interest

The authors declare that they have no known competing financial interests or personal relationships that could have appeared to influence the work reported in this paper.

Acknowledgements

The authors thank Dr. Tongyue Wang from the Laboratory of Light Environment at CAUP Tongji University for UVB irradiation system help and suggestion.

Appendix A. Supplementary data

Supplementary data to this article can be found online at https://doi.org/10.1016/j.heliyon.2024.e34321.

References

[1] L.R. Lorz, et al., Anti-wrinkling and anti-melanogenic effect of pradosia mutisii methanol extract, Int. J. Mol. Sci. 20 (5) (2019) 1043.
[2] T. Passeron, et al., Photoprotection according to skin phototype and dermatoses: practical recommendations from an expert panel, J. Eur. Acad. Dermatol. Venereol. 35 (7) (2021) 1460–1469.
[3] I. Rachmin, et al., Topical treatment strategies to manipulate human skin pigmentation, Adv. Drug Deliv. Rev. 153 (2020) 65–71.
[4] X. Zou, et al., Multi-omics analysis of an in vitro photoaging model and protective effect of umbilical cord mesenchymal stem cell-conditioned medium, Stem Cell Res. Ther. 13 (1) (2022) 435.
[5] Y. Zhang, et al., Circ_0011129 encapsulated by the small extracellular vesicles derived from human stem cells ameliorate skin photoaging, Int. J. Mol. Sci. 23 (23) (2022) 15390.
[6] V. Kostyuk, et al., Natural substances for prevention of skin photoaging: screening systems in the development of sunscreen and rejuvenation cosmetics, Rejuvenation Res. 21 (2) (2018) 91–101.
[7] S.H. Kwon, K.C. Park, Antioxidants as an epidermal stem cell activator, Antioxidants 9 (10) (2020) 958.
[8] H. Yang, et al., Facile solvent-free preparation of antioxidant idebenone-loaded nanoparticles for efficient wound healing, Pharmaceutics 14 (3) (2022) 521.
[9] J. Luo, et al., Anti-acne vulgaris effects of chlorogenic acid by anti-inflammatory activity and lipogenesis inhibition, Exp. Dermatol. 30 (6) (2021) 865–871.
[10] Y.C. Boo, Ascorbic acid (vitamin C) as a cosmeceutical to increase dermal collagen for skin antiaging purposes: emerging combination therapies, Antioxidants 11 (9) (2022) 1663.
[11] C.S. Yang, et al., Vitamin E and cancer prevention: studies with different forms of tocopherols and tocotrienols, Mol. Carcinog. 59 (4) (2020) 365–389.
[12] Y.Y. Chen, et al., Skin damage induced by zinc oxide nanoparticles combined with UVB is mediated by activating cell pyroptosis via the NLRP3 inflammasome-autophagy-exosomal pathway, Part. Fibre Toxicol. 19 (1) (2022) 2.
[13] Y. Zhou, et al., Combined topical and systemic administration with human adipose-derived mesenchymal stem cells (hADSC) and hADSC-derived exosomes markedly promoted cutaneous wound healing and regeneration, Stem Cell Res. Ther. 12 (1) (2021) 257.
[14] B. Zhao, et al., Human exosomes accelerate cutaneous wound healing by promoting collagen synthesis in a diabetic mouse model, Stem Cell. Dev. 30 (18) (2021) 922–933.
[15] Y. Zhou, et al., Human adipose-derived mesenchymal stem cells-derived exosomes encapsulated in pluronic F127 hydrogel promote wound healing and regeneration, Stem Cell Res. Ther. 13 (1) (2022) 407.
[16] Y. Fu, et al., Exosome lncRNA IFNG-AS1 derived from mesenchymal stem cells of human adipose ameliorates neurogenesis and ASD-like behavior in BTBR mice, J. Nanobiotechnol. 22 (1) (2024) 66.
[17] D. Bozic, et al., Conducting bioinformatics analysis to predict sulforaphane-triggered adverse outcome pathways in healthy human cells, Biomed. Pharmacother. 160 (2023) 114316.
[18] C. Schuster, et al., Combinatorial effects of the natural products arctigenin, chlorogenic acid, and cinnamaldehyde commit oxidation assassination on breast cancer cells, Antioxidants 11 (3) (2022).
[19] D.H. McDaniel, et al., Idebenone: a new antioxidant - Part I. Relative assessment of oxidative stress protection capacity compared to commonly known antioxidants, J. Cosmet. Dermatol. 4 (1) (2005) 10–17.
[20] R. Bengalli, et al., Safety assessment of polypyrrole nanoparticles and spray-coated textiles, Nanomaterials 11 (8) (2021) 1991.
[21] J. Park, et al., Protective effects of lanostane triterpenoids from chaga mushroom in human keratinocytes, HaCaT cells, against inflammatory and oxidative stresses, Int. J. Mol. Sci. 24 (16) (2023) 12803.
[22] J. Kim, et al., A novel multi-component formulation reduces inflammation in vitro and clinically lessens the symptoms of chronic eczematous skin, Int. J. Mol. Sci. 24 (16) (2023) 12979.
[23] E. Bang, D.H. Kim, H.Y. Chung, Protease-activated receptor 2 induces ROS-mediated inflammation through Akt-mediated NF-κB and FoxO6 modulation during skin photoaging, Redox Biol. 44 (2021) 102022.
[24] Y. Liu, et al., Glycyrol prevents the progression of psoriasis-like skin inflammation via immunosuppressive and anti-inflammatory actions, Int. J. Mol. Sci. 24 (24) (2023) 17335.
[25] C.Y. Zhang, et al., COX-2/sEH dual inhibitor alleviates hepatocyte senescence in NAFLD mice by restoring autophagy through Sirt1/PI3K/AKT/mTOR, Int. J. Mol. Sci. 23 (15) (2022) 8267.

[26] Y.J. Ahn, J.W. Lim, H. Kim, Docosahexaenoic acid induces expression of NAD(P)H: quinone oxidoreductase and heme oxygenase-1 through activation of Nrf2 in cerulein-stimulated pancreatic acinar cells, Antioxidants 9 (11) (2020) 1084.
[27] J. Shi, et al., IL-10 alleviates lipopolysaccharide-induced skin scarring via IL-10R/STAT3 axis regulating TLR4/NF-κB pathway in dermal fibroblasts, J. Cell Mol. Med. 25 (3) (2021) 1554–1567.
[28] T. Nacarelli, et al., NAD(+) metabolism governs the proinflammatory senescence-associated secretome, Nat. Cell Biol. 21 (3) (2019) 397–407.
[29] M. Watanabe, et al., Type XVII collagen coordinates proliferation in the interfollicular epidermis, Elife 6 (2017) e26635.
[30] S. Hiroyasu, et al., Granzyme B inhibition reduces disease severity in autoimmune blistering diseases, Nat. Commun. 12 (1) (2021) 302.
[31] E.A. Taha, et al., Knockout of MMP3 weakens solid tumor organoids and cancer extracellular vesicles, Cancers 12 (5) (2020) 1260.
[32] D. Xu, C. Li, M. Zhao, Theragra chalcogramma hydrolysate, rich in gly-leu-pro-ser-tyr-thr, alleviates photoaging via modulating deposition of collagen fibers and restoration of extracellular components matrix in SD rats, Mar. Drugs 20 (4) (2022) 252.
[33] J. Yang, et al., Rheological and mechanical analyses of felbinac cataplasms by using Box¯Behnken design, Pharmaceutics 10 (3) (2018) 88.
[34] V. Ievlev, et al., Krt14 and Krt15 differentially regulate regenerative properties and differentiation potential of airway basal cells, JCI Insight 8 (2) (2023) e162041.
[35] P. Wu, et al., HucMSC exosome-delivered 14-3-3ζ alleviates ultraviolet radiation-induced photodamage via SIRT1 pathway modulation, Aging (Albany NY) 13 (8) (2021) 11542–11563.
[36] H.J. Kim, et al., Augmentation of cellular NAD(+) by NQO1 enzymatic action improves age-related hearing impairment, Aging Cell 18 (5) (2019) e13016.
[37] Y.S. Park, et al., Inhibitory mechanism of ginsenoside Rh3 on granulocyte-macrophage colony-stimulating factor expression in UV-B-irradiated murine SP-1 keratinocytes, J Ginseng Res 44 (2) (2020) 274–281.
[38] Y. Shen, et al., Identification of master regulator genes of UV response and their implications for skin carcinogenesis, Carcinogenesis 40 (5) (2019) 687–694.
[39] A. Singh, et al., Exploring mycosporine-like amino acids (MAAs) as safe and natural protective agents against UV-induced skin damage, Antioxidants 10 (5) (2021) 683.
[40] W.S. Kim, et al., Mitochondria-targeted vitamin E protects skin from UVB-irradiation, Biomol Ther (Seoul) 24 (3) (2016) 305–311.
[41] H. Luiz, J. Oliveira Pinho, M.M. Gaspar, Advancing medicine with lipid-based nanosystems-the successful case of liposomes, Biomedicines 11 (2) (2023) 435.
[42] X. Liu, et al., Exosomes secreted from human-induced pluripotent stem cell-derived mesenchymal stem cells prevent osteonecrosis of the femoral head by promoting angiogenesis, Int. J. Biol. Sci. 13 (2) (2017) 232–244.
[43] J. Sanz-Ros, et al., Small extracellular vesicles from young adipose-derived stem cells prevent frailty, improve health span, and decrease epigenetic age in old mice, Sci. Adv. 8 (42) (2022) eabq2226.
[44] Y. Zhang, et al., Age-related changes in the inflammatory status of human mesenchymal stem cells: implications for cell therapy, Stem Cell Rep. 16 (4) (2021) 694–707.
[45] X. Zhao, et al., Chitosan hydrogel-loaded MSC-derived extracellular vesicles promote skin rejuvenation by ameliorating the senescence of dermal fibroblasts, Stem Cell Res. Ther. 12 (1) (2021) 196.
[46] P. Gentile, S. Garcovich, Adipose-derived mesenchymal stem cells (AD-MSCs) against ultraviolet (UV) radiation effects and the skin photoaging, Biomedicines 9 (5) (2021) 532.
[47] L. Yang, et al., FFAR4 improves the senescence of tubular epithelial cells by AMPK/SirT3 signaling in acute kidney injury, Signal Transduct. Targeted Ther. 7 (1) (2022) 384.
[48] T. Wang, et al., Overexpression of SIRT6 regulates NRF2/HO-1 and NF-κB signaling pathways to alleviate UVA-induced photoaging in skin fibroblasts, J. Photochem. Photobiol., B 249 (2023) 112801.
[49] A.Y. Kyadarkunte, M.S. Patole, V.B. Pokharkar, Cellular interactions and photoprotective effects of idebenone-loaded nanostructured lipid carriers stabilized using PEG-free surfactant, Int. J. Pharm. 479 (1) (2015) 77–87.
[50] S. Kawashima, et al., Protective effect of pre- and post-vitamin C treatments on UVB-irradiation-induced skin damage, Sci. Rep. 8 (1) (2018) 16199.
[51] F. Tan, et al., Clinical applications of stem cell-derived exosomes, Signal Transduct. Targeted Ther. 9 (1) (2024) 17.
[52] A.S. Pandey, D. Bawiskar, V. Wagh, Nanocosmetics and skin health: a comprehensive review of nanomaterials in cosmetic formulations, Cureus 16 (1) (2024) e52754.
[53] N. Hartman, J. Loyal, S. Fabi, Update on exosomes in aesthetics, Dermatol. Surg. 48 (8) (2022) 862–865.
[54] A.C. Franco, C. Aveleira, C. Cavadas, Skin senescence: mechanisms and impact on whole-body aging, Trends Mol. Med. 28 (2) (2022) 97–109.
[55] N. Liu, et al., Stem cell competition orchestrates skin homeostasis and ageing, Nature 568 (7752) (2019) 344–350.